Analysis of Electron Paramagnetic Resonance Spectra with Very Large Quadrupole Couplings

Neil G. Connelly,[†] David J. H. Emslie,[†] Phimphaka Klangsinsirikul,[†] and Philip H. Rieger*[,‡]

School of Chemistry, University of Bristol, Bristol BS8 1TS, U.K., and Department of Chemistry, Brown University, Providence, Rhode Island 02912

Received: August 1, 2002; In Final Form: October 14, 2002

Frozen solution electron paramagnetic resonance (EPR) spectra are reported for $[(\eta^4\text{-cod})Rh(\mu\text{-RNNNR})_2Ir(CO)_2]^+$ (cod = 1,5-cyclooctadiene), $[(PPh_3)(CO)Rh(\mu\text{-RNNNR})_2Ir(CO)(PPh_3)]^+$ (R = *p*-tolyl) and $[Tp'Ir(CO)(PPh_3]^+$ (Tp′ = hydrotris(3,5-dimethylpyrazolyl)borate). In the first spectrum, the Rh hyperfine coupling dominates and there are no significant quadrupolar effects. In the second spectrum, the low-field (g_x and g_y) features are 1:2:1 triplets rather than 1:1:1:1 quartets ($I = {}^3/_2$ for ^{191}Ir and ^{193}Ir), and in the third, the *x* and *y* features appear to be doublets. These anomalies result from the very large quadrupole moment for the iridium isotopes. This can be partially understood from a perturbation theory treatment, but quantitative simulations require direct matrix diagonalization and careful treatment of the problem, with respect to the orientation of the electron spin and nuclear spin quantization axes. The theoretical aspects of the calculations are presented, together with an interpretation of the results in terms of the electronic structures of the complexes.

Introduction

Frozen solution electron paramagnetic resonance (EPR) spectra have been generated recently showing quadrupolar effects that were previously unanticipated. Three spectra will be discussed in this paper, one of which does not show strange quadrupole effects. Two $[RhIr]^{3+}$ complexes are discussed:[1] $[(\eta^4\text{-cod})Rh(RNNNR)_2Ir(CO)_2]^+$ (cod = 1,5-cyclooctadiene) (**1**) and $[(PPh_3)(CO)Rh(RNNNR)_2Ir(CO)(PPh_3)]^+$ (R = *p*-tolyl) (**2**). The spectrum of **1**, shown in Figure 1a, shows only traces of quadrupole complications (most of the spin is apparently on the rhodium atom); that of **2**, Figure 2a shows major complications. The third spectrum, that of $[Tp'Ir(CO)(PPh_3)]^+$ (Tp′ = hydrotris(3,5-dimethylpyrazolyl)borate) (**3**) also shows major complications. ^{191}Ir (37.3%) and ^{193}Ir (62.7%) are both $I = {}^3/_2$ nuclei with comparable magnetic and quadrupole moments. For **2**, the high-field features are a doublet of quartets. In the spectrum of **2**, Figure 2a, the high-field features (g_z) constitute the expected quartet, albeit with a slightly larger than expected spacing between the $\pm{}^1/_2$ features, but the low-field (g_x) and middle-field (g_y) features are apparent 1:2:1 triplets. Coupling to ^{103}Rh ($I = {}^1/_2$) is observed on the high-field features in the spectrum of **2**. In the third spectrum, Figure 3a (related Rh(II) spectra have been reported[2]), the *x* and *y* features appear to be doublets, perturbed by hyperfine coupling to one ^{14}N nucleus, whereas the *z* features continue to be a quartet, complicated by coupling to one ^{14}N.

Peculiar line spacings have been reported previously for ^{197}Au ($I = {}^3/_2$) and ^{191,193}Ir spectra. There have been reports of quartets in dilute single-crystal spectra of Au complexes with smaller or larger central spacings,[3] but no analysis or interpretation was offered. An EPR spectrum of a Ir_2 complex analogous to 2 was reported[4] with the expected high-field septet, but with unequal spacings (the low-field and midfield features were not resolved). An EPR spectrum reported recently for an Ir(II)−ethene complex was very similar to that of 2,[5] but the authors assigned the low-field triplet to ^{1}H coupling, although they commented that the coupling was unusually large for protons. McDowell and co-workers[6] reported a spectrum with major quadrupole influence for ClSS. Most of the interest in quadrupolar effects in the past has been in the "forbidden" lines ($\Delta m_I \neq 0$), which become weakly allowed as a result of the quadrupole interaction.[7] No forbidden lines are resolved in the present spectra.

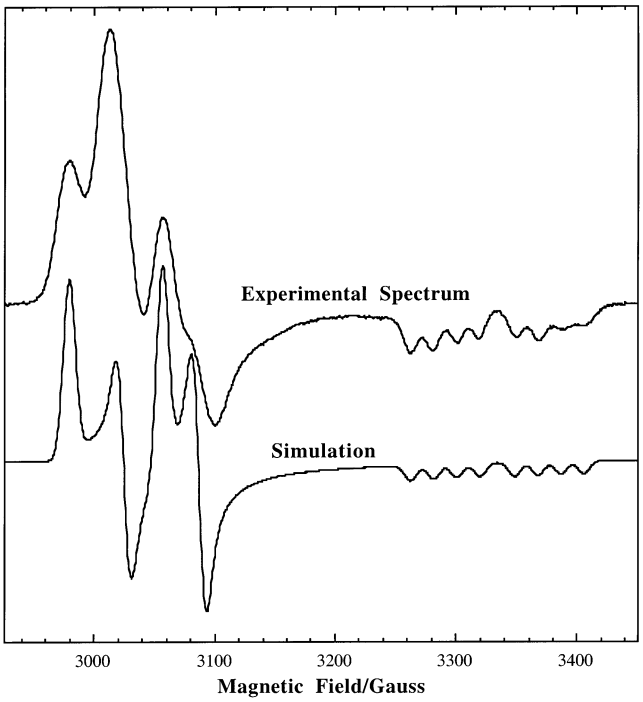

Figure 1. (a) Experimental X-band EPR spectrum of $[(\eta^4\text{-cod})Rh(RNNNR)_2Ir(CO)_2]^+$ (**1**) in CH_2Cl_2/thf at 100 K. (b) Computer simulation using parameters shown in Table 1.

[†] University of Bristol.
[‡] Brown University.

10.1021/jp021799z CCC: $22.00
Published on Web 12/03/2002

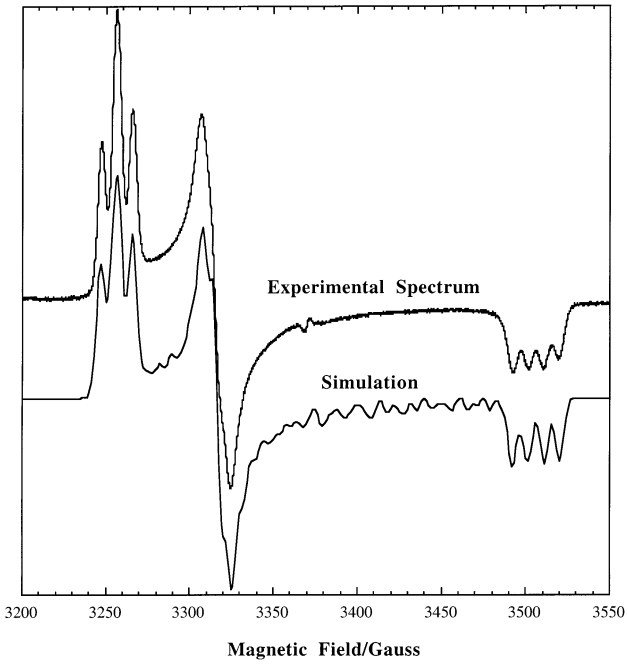

Figure 2. (a) Experimental X-band EPR spectrum of $[(PPh_3)(CO)Rh(RNNNR)_2Ir(CO)(PPh_3)]^+$ (**2**) in CH_2Cl_2/thf at 100 K. (b) Computer simulation using parameters shown in Table 1. Note that the (high-field) g_z features show a small coupling to ^{103}Rh ($I = {}^1/_2$) not included in the simulation.

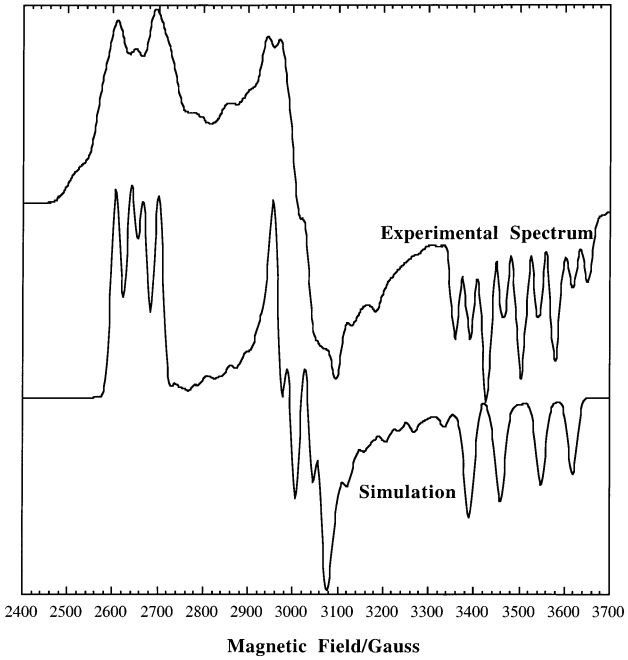

Figure 3. (a) Experimental X-band EPR spectrum of $[Tp'Ir(CO)(PPh_3)]^+$ (**3**) in $CH_2Cl_2/ClCH_2CH_2Cl$ at 100 K. (b) Computer simulation using parameters shown in Table 1. The ^{14}N hyperfine coupling is not included in the simulation.

The analysis in our earlier paper[4] was based on perturbation theory calculations.[8] The spectrum of 2 can be understood qualitatively in terms of the perturbation theory results. Given the spin Hamiltonian,

$$\boldsymbol{H} = \mu_B \vec{S}\cdot\bar{\bar{g}}\cdot\vec{B} + \vec{S}\cdot\bar{\bar{A}}\cdot\vec{I} + \vec{I}\cdot\bar{\bar{P}}\cdot\vec{I} \qquad (1)$$

where $\bar{P}$ is the quadrupole matrix with diagonal elements $-P(1-\eta)$, $-P(1+\eta)$, and $2P$. We assume that the $\bar{g}$ and $\bar{A}$ matrices share principal axes but that the quadrupole matrix $\bar{\bar{P}}$ may have principal axes displaced by the Euler angle α (rotation about z). The resonant fields are expected at

$$B = B_0 - \frac{mK}{g\mu_B} - \frac{F_1 m^2}{2g^2\mu_B{}^2 B} - \frac{F_2}{4g^2\mu_B{}^2 B}[I(I+1) - m^2] + \frac{8mF_3}{g\mu_B K}\left[I(I+1) - \left(2m^2 + \frac{1}{4}\right)\right] - \frac{mF_4}{g\mu_B K}\left[I(I+1) - \left(m^2 + \frac{1}{2}\right)\right]$$

where K is the angle-dependent hyperfine coupling

$$K^2 = \frac{1}{g^2}[A_{zz}{}^2 g_z{}^2 \cos^2\theta + (A_{xx}{}^2 g_x{}^2 \cos^2\varphi + A_{yy}{}^2 g_y{}^2 \sin^2\varphi)\sin^2\theta] \qquad (2)$$

(θ and ϕ describe the orientation of the magnetic field in the $\bar{\bar{g}}$ matrix principal axis system). F_1 and F_2 are second-order corrections arising from the hyperfine coupling term,

$$F_1(x) = \frac{A_x{}^4 g_x{}^2 - K^4}{g^2K^2} \qquad F_1(y) = \frac{A_y{}^4 g_y{}^2 - K^4}{g^2K^2} \qquad F_1(z) = \frac{A_z{}^4 g_z{}^2 - K^4}{g^2K^2}$$

$$F_2(x) = \frac{g_x{}^2 A_x{}^2 (A_z{}^2 + A_y{}^2)}{g^2K^2} \qquad F_2(y) = \frac{g_y{}^2 A_y{}^2 (A_z{}^2 + A_x{}^2)}{g^2K^2} \qquad F_2(z) = \frac{g_z{}^2 A_z{}^2 (A_y{}^2 + A_x{}^2)}{g^2K^2}$$

F_3 and F_4 arise from the quadrupole term,

$$F_3(x) = F_3(y) = P^2\eta^2(1 - \cos^2 2\alpha) \qquad F_3(z) = 0$$

$$F_4(x) = P^2[9 + 6\eta\cos 2\alpha + \eta^2\cos^2 2\alpha]$$

$$F_4(y) = P^2[9 - 6\eta\cos 2\alpha + \eta^2\cos^2 2\alpha]$$

$$F_4(z) = 4P^2\eta^2$$

Consider now the inner ($\pm{}^1/_2$) and outer ($\pm{}^3/_2$) quartet spacings (terms in F_1 and F_2 cancel):

$$\Delta B_{\text{outer}} = \frac{3K}{g\mu_B} + \frac{24F_3}{g\mu_B K} + \frac{3F_4}{g\mu_B K}$$

$$\Delta B_{\text{inner}} = \frac{K}{g\mu_B} - \frac{24F_3}{g\mu_B K} + \frac{3F_4}{g\mu_B K}$$

Assuming $\alpha = 45°$, F_3 and F_4 simplify to

$$F_3(x) = F_3(y) = P^2\eta^2 \qquad F_3(z) = 0$$

$$F_4(x) = F_4(y) = 9P^2 \qquad F_4(z) = 4P^2\eta^2$$

Under these circumstances, the inner and outer quartet spacings are

$$\Delta B_{\text{outer}}(x,y) = \frac{3K}{g\mu_B} + \frac{24P^2\eta^2}{g\mu_B K} + \frac{27P^2}{g\mu_B K}$$

$$\Delta B_{\text{inner}}(x,y) = \frac{K}{g\mu_B} - \frac{24P^2\eta^2}{g\mu_B K} + \frac{27P^2}{g\mu_B K}$$

$$\Delta B_{\text{outer}}(z) = \frac{K}{g\mu_B} + \frac{12P^2\eta^2}{g\mu_B K}$$

$$\Delta B_{\text{inner}}(z) = \frac{K}{g\mu_B} + \frac{12P^2\eta^2}{g\mu_B K}$$

From these expressions, it is clear that the outer spacing is expected to be less than 3 times the inner spacing for a field orientation along the z axis, but for orientations in the xy plane, the effect is reversed. However, to merge the two inner lines (to produce a 1:2:1 triplet), 24 $\eta^2 P$ would have to be comparable to K^2, and perturbation theory would fail, because the quadrupole coupling was treated as a perturbation on the hyperfine coupling problem. Accordingly, it was necessary to develop a program to diagonalize the Hamiltonian matrix.

In a first attempt, we took the Hamiltonian operator of eq 1, including the noncoincidence of the quadrupole and $\bar{g}$ matrix principal axes, computed matrix elements and diagonalized the matrix for 10 100 values of cos θ and ϕ and 250 values of B. The result was as might have been expected: quartets centered on the three g values. It is apparently necessary to take into careful account the quantization axes as was done in our perturbation theory treatment.

Theory

We start with the electron Zeeman term, $\mu_B \vec{S}\cdot\bar{\bar{g}}\cdot\vec{B}$, where $\vec{S}$ is quantized along $\bar{\bar{g}}\cdot\vec{B}$, i.e., $\vec{S}\cdot\bar{\bar{g}}\cdot\vec{B} = gBS_{z'}$. Thus there must be a transformation matrix $\bar{\bar{Q}}$ which, applied to $\bar{\bar{g}}\cdot\vec{B}$, gives

$$\bar{\bar{Q}}\cdot\bar{\bar{g}}\cdot\vec{B} = \bar{\bar{Q}}\cdot\begin{pmatrix} g_x B\sin\theta\cos\phi \\ g_x B\sin\theta\cos\phi \\ g_z B\cos\theta \end{pmatrix} = \begin{pmatrix} 0 \\ 0 \\ gB \end{pmatrix}$$

where Q is written in terms of the Euler angles, ζ, ξ, and χ:[9]

$$\bar{\bar{Q}} = \begin{bmatrix} \cos\zeta\cos\xi\cos\chi - \sin\zeta\sin\chi & \sin\zeta\cos\xi\cos\chi + \cos\zeta\sin\chi & -\sin\xi\cos\chi \\ -\cos\zeta\cos\xi\sin\chi - \sin\zeta\cos\chi & -\sin\zeta\cos\xi\sin\chi + \cos\zeta\cos\chi & \sin\xi\sin\chi \\ \cos\zeta\sin\xi & \cos\zeta\sin\xi & \cos\xi \end{bmatrix}$$

In the $\bar{\bar{g}}$ matrix principal axis system, B can be written

$$B = B_x\sin\theta\cos\phi + B_y\sin\theta\sin\phi + B_z\cos\theta$$

it is easily shown that

$$\cos\zeta = \frac{g_x}{g_\perp\cos\phi} \qquad \sin\zeta = \frac{g_y}{g_\perp}\sin\phi$$

$$\cos\xi = \frac{g_z}{g}\cos\theta \qquad \sin\xi = \frac{g_\perp}{g}\sin\theta$$

where $g_\perp{}^2 = g_x{}^2\cos^2\phi + g_y{}^2\sin^2\phi$ and $g^2 = g_\perp{}^2\sin^2\theta + g_y{}^2\cos^2\theta$. The angle χ is left indeterminant, equivalent to saying that the x and y components of S are not fixed in space. As it happens, this has no consequences for either the perturbation theory treatment or the full matrix diagonalization treatment where χ must be given a value, but the results are independent of the value chosen.

Turning to the nuclear spin, we assume that the nuclear spin is quantized along the hyperfine field.[10] At this point, we have three coordinate systems. The $\bar{\bar{g}}$ and $\bar{\bar{A}}$ matrix principal axes (x, y, z), the electron-spin quantization axes (x', y', z') and the nuclear-spin quantization axes (x'', y'', z''). In the x', y', z' system, the hyperfine term can be written

$$\vec{S}\cdot\bar{\bar{Z}}\cdot\vec{I} = S_{x'}(Z_{11}I_{x'} + Z_{12}I_{y'} + Z_{13}I_{z'}) + S_{y'}(Z_{21}I_{x'} + Z_{22}I_{y'} + Z_{23}I_{z'}) + S_{z'}(Z_{31}I_{x'} + Z_{32}I_{y'} + Z_{33}I_{z'}) \quad (3)$$

where

$$\bar{\bar{Z}} = \bar{\bar{Q}}^{-1}\cdot\bar{\bar{A}}\cdot\bar{\bar{Q}}$$

$$Z_{11} = \frac{(A_{xx}g_z{}^2\cos^2\varphi + A_{yy}g_y{}^2\sin^2\varphi)g_z{}^2\cos^2\theta + A_{zz}g_\perp{}^4\sin^2\theta}{g^2g_\perp{}^2}$$

$$Z_{22} = \frac{A_{xx}g_y{}^2\sin^2\varphi + A_{yy}g_x{}^2\cos^2\varphi}{g^2g_\perp{}^2}$$

$$Z_{33} = \frac{(A_{xx}g_x{}^2\cos^2\varphi + A_{yy}g_y{}^2\sin^2\varphi)\sin^2\theta + A_{zz}g_z{}^2\cos^2\theta}{g^2}$$

$$Z_{21} = Z_{12} = \frac{(A_{yy} - A_{xx})g_xg_yg_z\cos\theta\cos\varphi\sin\varphi}{gg_\perp{}^2}$$

$$Z_{31} = Z_{13} = \frac{(A_{xx}g_x{}^2\cos^2\varphi + A_{yy}g_y{}^2\sin^2\varphi - A_{zz}g_\perp{}^2)g_z\sin\theta\cos\theta}{g^2g_\perp}$$

$$Z_{23} = Z_{32} = \frac{(A_{yy} - A_{xx})g_xg_y\sin\theta\sin\varphi\cos\varphi}{gg_\perp}$$

The last term in eq 3 reduces to $KS_{z'}I_{z''}$ when we write I in the x'', y'', z'' system, where K is given by eq 2. This is equivalent to operating on I written in the x', y', z' system with a tranformation matrix with Euler angles κ, λ, and μ. Two of the angles are determined:

$$\cos\kappa\sin\lambda = Z_{31}/K \qquad \sin\kappa\sin\lambda = Z_{32}/K \qquad \cos\lambda = Z_{33}/K$$

The third Euler angle μ remains indeterminant. This makes no difference for a perturbation theory treatment, and we have shown for a variety of arbitrarily chosen angles that μ has no effect on the matrix diagonalization method, and our simulation program simply sets $\mu = 0$. Matrix elements of the electron Zeeman and nuclear hyperfine terms of the spin Hamiltonian are given in the Appendix.

The quadrupole interaction term in the spin Hamiltonian is

$$\vec{I}\cdot\begin{pmatrix} -\eta P\cos 2\alpha - P & \eta P\sin 2\alpha & 0 \\ \eta P\sin 2\alpha & \varphi P\cos 2\alpha - P & 0 \\ 0 & 0 & 2P \end{pmatrix}\cdot\vec{I}$$

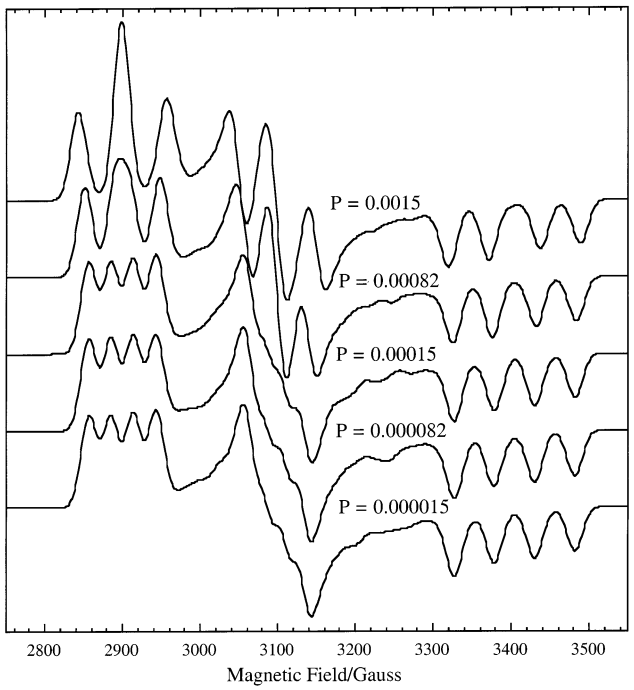

Figure 4. Simulations with g and A^{Ir} from Table 1 (**2**), $\alpha = 45°$, $\eta = 5000$, and P ranging from 0.000 015 to 0.0015 ($\times 10^{-4}$ cm^{-1}).

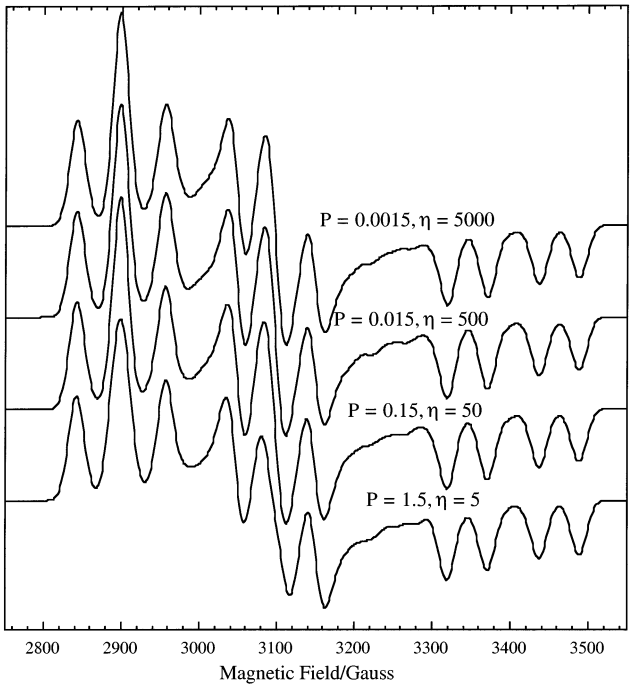

Figure 5. Simulations with g and A^{Ir} from Table 1 (**2**), $\alpha = 45°$, $P\eta = 7.5$ ($\times 10^{-4}$ cm^{-1}), and η ranging from 5 to 5000.

Transformed to the x'',y'',z'' system, the matrix must remain symmetric and traceless:

$$\vec{I}\cdot\bar{P}\cdot\vec{I} = (I_{x''}I_{y''}I_{z''})\begin{pmatrix} P_{11} & P_{12} & P_{13} \\ P_{12} & P_{22} & P_{23} \\ P_{13} & P_{23} & P_{33} \end{pmatrix}\begin{pmatrix} I_{x''} \\ I_{y''} \\ I_{z''} \end{pmatrix}$$

$$\vec{I}\cdot\bar{P}\cdot\vec{I} = P_{33}I_{z''}^2 - \frac{1}{4}P_{33}(I_+I_- + I_-I_+)$$

$$+ \frac{1}{2}(P_{13} + iP_{23})(I_-I_z + I_zI_-) + \frac{1}{2}(P_{13} - iP_{23})(I_+I_z + I_zI_+) -$$

$$\frac{i}{2}P_{12}(I_+^2 - I_-^2) + \frac{1}{4}(P_{11} - P_{22})(I_+^2 + I_-^2)$$

Given the transformation matrix based on the Euler angles κ and λ, the P_{ij} components are easily computed; The matrix elements of the quadrupole term of the spin Hamiltonian are then easily computed and are given in the Appendix.

Given a simulation program, we can investigate the conditions under which a 1:1:1:1 quartet is converted to a 1:2:1 triplet or a 1:1 doublet. Shown in Figure 4 are simulations using parameters appropriate to **2** for $\eta = 5000$ and P ranging from 0.000 015 to 0.0015 ($\times 10^{-4}$ cm^{-1}). Note that the small peaks between the major features in Figure 4 (and other simulations) are due to an insufficient number of angles. For $P < 0.00082$, the x features are a quartet (the y features are poorly resolved, but would also be a quartet for narrower lines). For $P = 0.000\,82$, the two central lines of the quartet are nearly merged, and for $P = 0.0015$, the merger is complete. Figure 5 shows a series of simulations for constant $P\eta = 7.5$, but with variable P and η. Here we see that the simulation is nearly independent of the values of P and η for a given product; however, because $P\eta \gg 2P$, the quadrupole effect is largely in the xy plane. Figure 6 shows a series of simulations for variable α, the Euler angle rotating the principal axes of the quadrupole interaction matrix. Here we see that α must be on the order of 45° to produce a 1:2:1 triplet, exactly as predicted by our perturbation theory calculations.

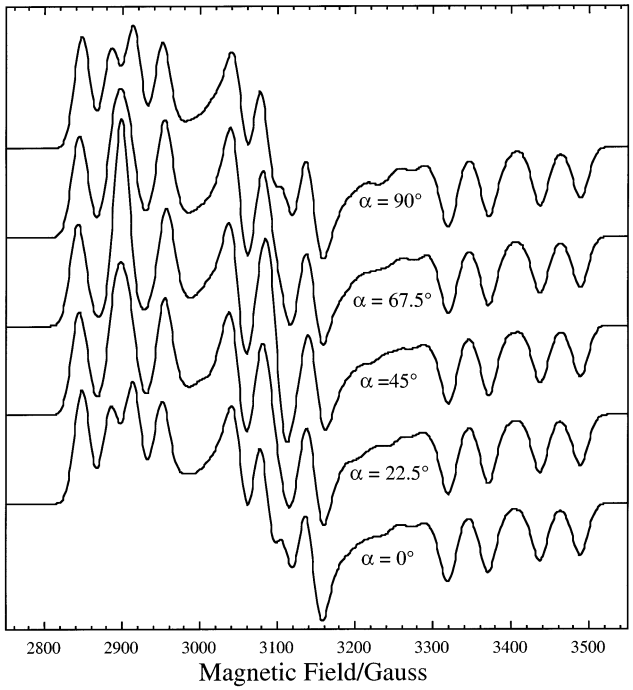

Figure 6. Simulations with g and A^{Ir} from Table 1 (**2**), $P = 0.0015$ ($\times 10^{-4}$ cm^{-1}), $\eta = 5000$, and α ranging from 0 to 90°.

The spectrum of **3** appears to have a 1:1 doublet as the low-field feature, rather than a triplet. This was at first quite puzzling, because this cannot be predicted from perturbation theory. In the course of exploring the parameter space, however, we found that for small hyperfine couplings, doublets (and quartets) are indeed found. Indeed, the doublet results when the outer quartet splitting is unresolved. This effect is shown in Figure 7 for $A_x = A_y$ varying from 10 to 30 ($\times 10^{-4}$ cm^{-1}).

The $\bar{\bar{g}}$ components are accurately found from the average fields of the three sets of components from each spectrum. First estimates of the hyperfine coupling components can be obtained from the 1:2:1 triplet spacings for **1**, but some refinement is

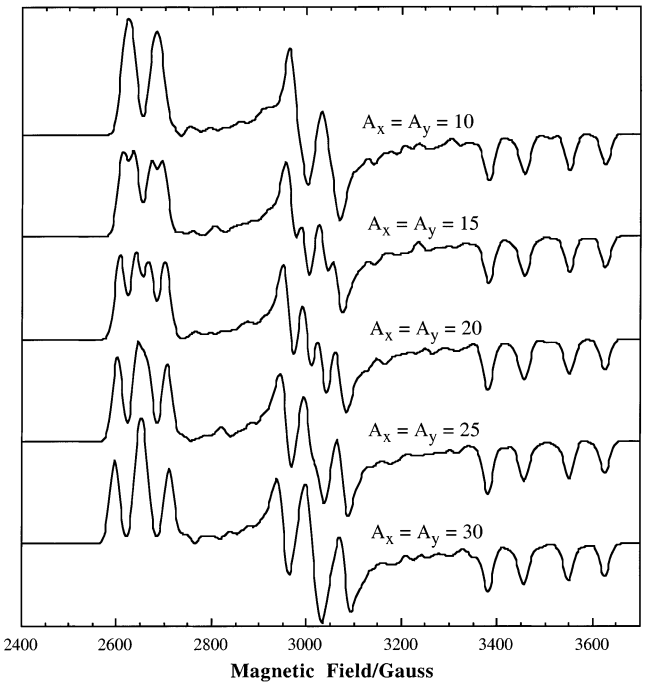

Figure 7. Simulations with g and A_z^{Ir} from Table 1 (**3**), $P = 0.5$, $\eta = 20$, $\alpha = 45°$, and A_x and A_y ranging from 10 to 30 ($\times 10^{-4}$ cm^{-1}).

TABLE 1: Best-Fit Parameters for 1−3

	1	2	3
g	2.236, 2.208, 2.024	2.3273, 2.1772, 1.9821	2.544, 2.238, 1.927
A^a	(Rh) 80.6, 64.3, 81.0	(Ir) 31.3, 22.8, 47.4	(Ir) 20, 15, 62.5
	(Ir) —, —, 18.0	(Rh) —, —, 16.6	(N) ca. 80, ca. 40, 29.5
P*	($\eta P = 1.0$)	0.0015	0.5
η		5000	20
α		45°	45°

[a] $\times 10^{-4}$ cm^{-1}.

necessary when the fit is nearly right because the spacing of the features depends somewhat on the quadrupole parameters. The quadrupole parameters are best fitted by starting with estimates from perturbation theory. The best fit parameters are given in Table 1, and simulations based on these parameters are shown in Figures 1b and 2b for **1** and **2**, respectively.

Results

Consider first the Rh−Ir complex, **1**. From the z components, $\eta P = 1.0$, but because there is no resolved Ir hyperfine structure on the x and y components, we can go no further in analyzing the quadrupole effects. The $\bar{\bar{g}}$ and $\bar{\bar{A}}$ components are given in Table 1. The isotropic spectrum was not well resolved so we cannot quote with certainty an isotropic Rh hyperfine coupling. From previous work on Rh_2 analogues,[11] we expect the Rh and Ir contributions to the singly occupied MO (SOMO) will be primarily d_{z^2} with some $d_{x^2-y^2}$ admixture. With $P = -40.4 \times 10^{-4}$ cm^{-1} for ^{103}Rh,[12] the dipolar hyperfine contributions are

$$A_{xx} = \frac{2}{7}P(-c_{z^2}{}^2 + c_{x^2-y^2}{}^2 - 2\sqrt{3}c_{z^2}c_{x^2-y^2})$$

$$A_{yy} = \frac{2}{7}P(-c_{z^2}{}^2 + c_{x^2-y^2}{}^2 + 2\sqrt{3}c_{z^2}c_{x^2-y^2})$$

$$A_{zz} = \frac{4}{7}P(c_{z^2}{}^2 - c_{x^2-y^2}{}^2)$$

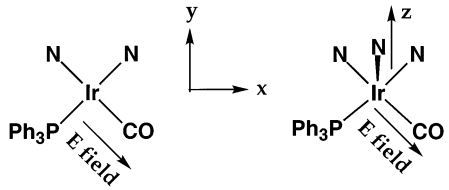

Figure 8. Coordination geometry of Ir in **2** and **3**.

If we assume the measured hyperfine components all have the same sign, we have $\langle A \rangle = 75.3 \times 10^{-4}$ cm^{-1}, and $c_{z^2}{}^2 = 0.361$, $c_{x^2-y^2}{}^2 = 0.115$ for a total Rh contribution to the SOMO of 0.476. The Ir contribution is apparently considerably smaller. Other sign assumptions lead to $c_{z^2}{}^2 \gg 1$.

The other Rh−Ir complex, **2**, is another matter altogther. From the z components, $\eta P = 1.4 \pm 0.9$, but simulations showed that $\eta P = 7.5$ gives a better fit. Best-fit EPR parameters are given in Table 1. The isotropic spectrum again was unresolved, so we cannot be sure of relative signs of the hyperfine components, but again we are forced to conclude that all hyperfine components have the same sign, $\langle A \rangle = 33.85 \times 10^{-4}$ cm^{-1}. Thusthe dipolar contributions are -2.57, -11.02, and $+13.60$ ($\times 10^{-4}$ cm^{-1}). These are consistent with the $d_{z^2}/d_{x^2-y^2}$ SOMO found in previous work on Rh_2 complexes.[11] With $P = 39.8 \times 10^{-4}$ cm^{-1} (weighted average of two Ir isotopes).[12] we get $c_{z^2}{}^2 = 0.617$, $c_{x^2-y^2}{}^2 = 0.019$ for a total Ir contribution to the SOMO of 0.636. This result is consistent with the small Rh hyperfine coupling. The large quadrupole effect is consistent with the coordination environment of the Ir nucleus, as shown in Figure 8. The principal axes of the $\bar{\bar{g}}$ matrix are determined by molecular symmetry. All ligands are primarily σ-donors except CO which is also a π-acceptor. Thus we expect an electric field gradient in the direction of the CO, 45° away from the x axis, as determined in the EPR analysis.

Turning to $[Tp'Ir(CO)(PPh_3)]^+$, **3**, the spectrum can be understood as well-separated x, y, and z components (from low to high field). The low-field and middle-field features (x and y) appear to be quartets with superimposed ^{14}N triplets. In the case of the x components, a^N is on the order of the $\pm^3/_2$ splitting; for the y components, a^N is approximately equal to the $\pm^1/_2$ splitting. The z components consist of the expected iridium quartet with a^N on the order of half the quartet splitting. We must recognize that the parameter estimates given in Table 1 are not very reliable because there is a large interaction between the hyperfine and quadrupolar parameters in determining the doublet spacings for the x and y components. On the basis of the analogous rhodium complexes, we expect the SOMO to be primarily metal d_{z^2} (consistent with the single ^{14}N coupling). The Ir hyperfine couplings are not quite right in that they suggest more than one unpaired electron if we assume a $d_{z^2}/d_{x^2-y^2}$ SOMO.′ It is not surprising that the quadrupole coupling would be large and largely confined to the xy plane, because again there is a π-acceptor CO ligand leading to an electric field gradient at the iridium nucleus as shown in Figure 8.

Experimental Section

Preparation of Samples. *[(η^4-cod)Rh(μ-p-MeC$_6$H$_4$NNN-C$_6$H$_4$Me-p)$_2$Ir(CO)$_2$][PF$_6$]·0.5CH$_2$Cl$_2$ (**1**).* To a deep red solution of [(η^4-cod)Rh(p-MeC$_6$H$_4$NNNC$_6$H$_4$Me-p)$_2$Ir(CO)$_2$][1] (0.056 g, 0.06 mmol) in CH_2Cl_2 (15 cm^3) was added $AgPF_6$ (0.015 g, 0.06 mmol). After 2 min the red-brown solution was filtered through Celite, n-hexane (15 cm^3) was added, and the mixture was reduced in volume to give a red-brown solid, yield 61 mg

(90%). Anal. Calcd (Found): C, 42.8 (42.2); H, 3.8 (3.8); N, 7.8 (7.7). IR (CH_2Cl_2): ν(CO) 2089, 2040 cm^{-1}.

*[(CO)(Ph$_3$P)Rh(μ-p-MeC$_6$H$_4$NNNC$_6$H$_4$Me-p)$_2$Ir(CO)(PPh$_3$)][PF$_6$]·1.5CH$_2$Cl$_2$ (**2**).* To a dark purple solution of [$(CO)_2$Rh(μ-p-$MeC_6H_4NNNC_6H_4$Me-p)$_2$Ir$(CO)_2$][1] (0.051 g, 0.06 mmol) in CH_2Cl_2 (20 cm^3) was added PPh_3 (0.031 g, 0.12 mmol). After 5 min [Fe(η-C_5H_5)$_2$][PF_6] (0.020 g, 0.06 mmol) was added to the dark red solution. The orange-brown solution was stirred for 10 min and then evaporated to dryness in vacuo. The golden orange solid was washed with *n*-hexane (5 × 20 cm^3). The complex was further purified by allowing a concentrated CH_2Cl_2 solution of the complex to diffuse slowly into *n*-hexane to give orange crystals, yield 0.081 g (92%). Anal. Calcd (Found): C, 51.1 (50.8); H, 3.2 (3.8); N, 5.4 (5.3). IR (CH_2Cl_2): ν(CO) 2043, 2010 cm^{-1}.

*[Tp′Ir(CO)(PPh3)] (**3**).* Ethene was bubbled through a degassed (three freeze−pump−thaw cycles) suspension of [{Ir(cyclooctene)$_2$(μ-Cl)}$_2$][13] (250 mg, 0.28 mmol) in thf (10 cm^3) until the solution color remained constant. Upon addition of a solution of KTp′ [14] (202 mg, 0.60 mmol) in thf (5 cm^3) by cannula, the color changed from yellow to dark red and then green-brown (with the formation of [Ir$(C_2H_4)_2$Tp′].[15] At this point, a solution of PPh_3 (150 mg, 0.57 mmol) in thf (5 cm^3) was added by cannula to give a red-brown solution of [Ir(C_2H_4)(PPh$_3$)Tp′].[16] After the mixture was stirred for 1 h, CO was bubbled through the solution for 1 min to yield a bright yellow solution which was stirred under nitrogen for 3 days. The mixture of products was adsorbed onto silica and applied to a silica−*n*-hexane chromatography column. Impurities were removed by increasing the proportion of Et_2O in *n*-hexane until, in 100% Et_2O, a bright yellow band containing only three components (by IR spectroscopy) was eluted. This was evaporated to dryness in vacuo to give an oily yellow solid that was dissolved in the minimum volume of hot *n*-hexane (ca. 130 cm^3) and stored at −10 °C for 2 days. The pale yellow mother liquors were decanted from the bright yellow powder that was dried in vacuo, yield 56 mg (13%). Anal. Calcd (Found): C, 52.0 (52.4); H, 4.7 (4.8); N, 10.4 (10.8). IR (CH_2Cl_2): ν(CO) 1964 cm^{-1}. Complex **3** is reversibly oxidized at $E^\circ = 0.06$ V at a glassy carbon electrode; the oxidation wave becomes severely broadened at a platinum electrode.

EPR Spectroscopy. Complex **1** decomposes within a few days. It was therefore freshly prepared, placed as a solid in an EPR tube, and dissolved in a mixture of thf−CH_2Cl_2 (2:1). Complex **2** is stable; a pure crystalline sample was therefore dissolved in a mixture of thf−CH_2Cl_2 (2:1) to obtain the EPR spectra. [Ir(CO)(PPh$_3$)Tp′][PF_6], **3**, a rare example of an iridium(II) complex was generated in situ by reacting the neutral complex **3** with [$FeCp_2$][PF_6] at 220 K in a 1:1 mixture of CH_2Cl_2−1,2-dichloroethane. The mixture was then cooled to between 100 and 120 K to obtain an anisotropic spectrum.

X-band EPR spectra were recorded on a Bruker 300ESP spectrometer equipped with a Bruker variable temperature accessory and a Hewlett-Packard 5350B microwave frequency counter. The field calibration was checked by measuring the resonance of the diphenylpicrylhydrazyl radical before each series of spectra.

Appendix. Matrix Elements

Matrix elements arising from the quadrupole term of the spin Hamiltonian:

$$\langle I,m|H_Q|I,m\rangle = \frac{1}{2}P_{33}[3m^2 - I(I+1)]$$

$$\langle I,m-1|H_Q|I,m\rangle = \frac{1}{2}(P_{13} + iP_{23})(2m-1)\sqrt{I(I+1) - m(m-1)}$$

$$\langle I,m+1|H_Q|I,m\rangle = \frac{1}{2}(P_{13} - iP_{23})(2m+1)\sqrt{I(I+1) - m(m-1)}$$

$$\langle I,m+2|H_Q|I,m\rangle = \frac{1}{4}(P_{11} - P_{22} - 2iP_{12})\sqrt{[I(I+1) - (m+1)^2]^2 - (m+1)^2}$$

$$\langle I,m-2|H_Q|I,m\rangle = \frac{1}{4}(P_{11} - P_{22} - 2iP_{12})\sqrt{[I(I+1) - (m-1)^2]^2 - (m-1)^2}$$

Matrix elements arising from the electron Zeeman and nuclear hyperfine interaction terms of the spin Hamiltonian:

$$\left\langle \frac{1}{2},m_S;I,m_I\middle|H_s\middle|\frac{1}{2},m_S;I,m_I\right\rangle = m_S g\mu_B B + m_S m_I K$$

$$\left\langle \frac{1}{2},-\frac{1}{2};I,m_I\middle|H_s\middle|\frac{1}{2},\frac{1}{2};I,m_I\right\rangle = \frac{m_I}{2}(Fx + iFy)$$

$$\left\langle \frac{1}{2},\frac{1}{2};I,m_I\middle|H_s\middle|\frac{1}{2},-\frac{1}{2};I,m_I\right\rangle = \frac{m_I}{2}(Fx - iFy)$$

$$\left\langle \frac{1}{2},-\frac{1}{2};I,m_I-1\middle|H_s\middle|\frac{1}{2},\frac{1}{2};I,m_I\right\rangle = \frac{1}{4}[(D_x - E_y) + i(D_y + E_x)]\sqrt{I(I+1) - m_I(m_I-1)}$$

$$\left\langle \frac{1}{2},-\frac{1}{2};I,m_I+1\middle|H_s\middle|\frac{1}{2},\frac{1}{2};I,m_I\right\rangle = \frac{1}{4}[(D_x + E_y) + i(D_y - E_x)]\sqrt{I(I+1) - m_I(m_I+1)}$$

$$\left\langle \frac{1}{2},\frac{1}{2};I,m_I+1\middle|H_s\middle|\frac{1}{2},-\frac{1}{2};I,m_I\right\rangle = \frac{1}{4}[(D_x - E_y) - iD_y + E_x)]\sqrt{I(I+1) - m_I(m_I+1)}$$

$$\left\langle \frac{1}{2},\frac{1}{2};I,m_I-1\middle|H_s\middle|\frac{1}{2},-\frac{1}{2};I,m_I\right\rangle = \frac{1}{4}[(D_x + E_y) - i(D_y - E_x)]\sqrt{I(I+1) - m_I(m_I-1)}$$

where K is given by eq 2 and

$$F_x = -Z_{11}\sin\kappa + Z_{13}\cos\kappa$$

$$F_y = -Z_{21}\sin\kappa + Z_{23}\cos\kappa$$

$$D_x = Z_{11}\cos\lambda\cos\kappa - Z_{12}\sin\lambda + Z_{13}\cos\lambda\sin\kappa$$

$$D_y = Z_{21}\cos\lambda\cos\kappa - Z_{22}\sin\lambda + Z_{23}\cos\lambda\sin\kappa$$

$$E_x = Z_{11}\sin\lambda\cos\kappa + Z_{12}\cos\lambda + Z_{13}\sin\lambda\sin\kappa$$

$$E_y = Z_{21}\sin\lambda\cos\kappa + Z_{22}\cos\lambda + Z_{23}\sin\lambda\sin\kappa$$

Acknowledgment. We thank Dr. David Collison of the University of Manchester for help with the simulation program and Prof. Richard Stratt of Brown University for helpful suggestions regarding the indeterminant angles.

References and Notes

(1) Connelly, N. G.; Hayward, O. D.; Klangsinsirikul, P.; Orpen, A. G.; Rieger, P. H. *Chem. Commun.* **2000**, 963.

(2) Connelly, N. G.; Emslie, D. J. H.; Geiger, W. E.; Hayward, O. D.; Linehan, E. B.; Orpen, A. G.; Quayle, M. J.; Rieger, P. H. *J. Chem. Soc., Dalton Trans.* **2001**, 670.

(3) (a) van Rens, J. G. M.; de Boer, E. *Mol. Phys.* **1970**, *19*, 745. (b) van Rens, J. G. M.; Viegers, M. P. A.; de Boer, E. *Chem. Phys. Lett.* **1974**, *28*, 104. (c) Ihlo, L.; Böttcher, R.; Olk, R.-M.; Kirmse, R. *Inorg. Chim. Acta* **1998**, *281*, 160.

(4) DeGray, J. A.; Rieger, P. H.; Connelly, N. G.; Garcia Herbosa, G. *J.* Magn. Reson. **1990**, *88*, 376.

(5) de Bruin, B.; Peters, T. P. J.; Thewissen, S.; Blok, A. N. J.; Wilting, J. B. M.; de Gelder, R.; Smits, J. M. M.; Gal, A. W. *Angew. Chem., Int. Ed.* **2002**, *41*, 2135.

(6) Herring, F. G.; McDowell, C. A.; Tait, J. C. *J. Chem. Phys.* **1972**, *57*, 4564.

(7) (a) Keijzers, C. P.; Paulussen, G. F. M.; de Boer, E. *Mol. Phys.* **1975**, *29*, 973. (b) Belford, R. L.; Duan, D. C. *J.* Magn. Reson. **1978**, *29*, 293. (c) Netter, D.; Villafranca, J. J. *J.* Magn. Reson. **1985**, *64*, 61.

(8) DeGray, J. A. Ph.D. Thesis, Brown University, 1987.

(9) Wilson, E. B.; Decius, J. C.; Cross, P. C. *Molecular Vibrations*; McGraw-Hill: New York, 1955; p 286. Watanabe, H. *Operator Methods in Ligand Field Theory*; Prentice-Hall: Englewood Cliffs, NJ, 1966; p 147.

(10) Blinder, S. M. *J. Chem. Phys.* **1960**, *33*, 748.

(11) Boyd, D. C.; Connelly, N. G.; Herbosa, G. G.; Hill, M. G.; Mann, K. R.; Mealli, C.; Orpen, A. G.; Richardson, K. E.; Rieger, P. H. *Inorg. Chem.* **1994**, *33*, 960.

(12) Morton, J. R.; Preston, K. F. *J. Magn. Reson.* **1978**, *30*, 577.

(13) van der Ent, A.; Onderdelinden, A. L. *Inorg. Synth.* **1990**, *28*, 90.

(14) Trofimenko, S. *Inorg. Synth.* **1970**, *12*, 99.

(15) Tanke, R. S.; Crabtree, R. H. *Inorg. Chem.* **1989**, *28*, 3444.

(16) Gutiérrez-Puebla, E.; Monge, A.; Nicasio, M. C.; Pérez, P. J.; Poveda, M. L.; Rey, L.; C. Ruíz, C.; Carmona, E. *Inorg. Chem.* **1998** *37*, 4538; Oldham, W. J., Jr.; Heinekey, D. M. *Organometallics* **1997**, *16*, 467.